Differences in *orthodenticle* expression promote ommatidial size variation between *Drosophila* species

Montserrat Torres-Oliva[1,2,*], Elisa Buchberger[1,*], Alexandra D. Buffry[3,*], Maike Kittelmann[3], Lauren Sumner-Rooney[4], Pedro Gaspar[3,5], Georg C. Bullinger[1], Genoveva Guerrero[6], Fernando Casares[6], Saad Arif[3,§], Nico Posnien[1,§], Maria D. S. Nunes[3,§], Alistair P. McGregor[3, §] and Isabel Almudi[3,6, §]

1. University Göttingen, Department of Developmental Biology, Justus-von-Liebig-Weg 11, 37077 Göttingen, Germany
2. Current address: Institute of Clinical Molecular Biology, Christian-Albrechts-University of Kiel, University Hospital Schleswig-Holstein, Kiel, Germany
3. Department of Biological and Medical Sciences, Oxford Brookes University, Oxford, OX3 0BP, UK.
4. Oxford University Museum of Natural History, Parks Road, Oxford OX1 3PW, UK.
5. MRC London Institute of Medical Sciences, London W12 0NN, UK.
6. Present address GEM-DMC2 Unit, CABD (CSIC-UPO-JA), Ctra. de Utrera km 1, 41013 Seville, Spain

*Contributed equally

§ Corresponding authors

Key words: compound eyes, ommatidia, *Drosophila*, evolution, heterochrony, development, *orthodenticle*.

Abstract

The compound eyes of insects exhibit extensive variation in ommatidia number and size, which affects how they see and underlies adaptations in their vision to different environments and lifestyles. However, very little is known about the genetic and developmental bases underlying differences in compound eye size. We previously showed that the larger eyes of *Drosophila mauritiana* compared to *D. simulans* is caused by differences in ommatidia size rather than number. Furthermore, we identified an X-linked chromosomal region in *D. mauritiana* that results in larger eyes when introgressed into *D. simulans*. Here, we used a combination of fine-scale mapping and gene expression analysis to further investigate positional candidate genes on the X chromosome. We found that *orthodenticle* is expressed earlier in *D. mauritiana* than in *D. simulans* during ommatidial maturation in third instar larvae, and we further show that this gene is required for the correct organisation and size of ommatidia in *D. melanogaster*. Using ATAC-seq, we have identified several candidate eye enhancers of *otd* as well as potential direct targets of this transcription factor that are differentially expressed between *D. mauritiana* and *D. simulans*. Taken together, our results suggest that differential timing of *otd* expression contributes to natural variation in ommatidia size between *D. mauritiana* and *D. simulans,* which provides new insights into the mechanisms underlying the regulation and evolution of compound eye size in insects.

Introduction

Understanding the genetic and genomic basis of phenotypic diversity is one of the central themes of evolutionary biology. While the causative genes and even mutations have been identified underlying evolutionary changes in a growing list of phenotypes (e. g. (Arif et al., 2013; Arnoult et al., 2013; Hagen et al., 2019; Klaassen et al., 2018; Ramaekers et al., 2019; Santos et al., 2017) and see (Courtier-Orgogozo et al., 2019) for a more comprehensive list) we still know relatively little about the genetic basis for the evolution of organ size. Identifying such genes will not only broaden our understanding of morphological change but provide further insights into the mechanisms underlying the control of organ size.

Insects exhibit remarkable variation in the size and shape of their compound eyes, which has allowed these animals to adapt to different environments and lifestyles (Land and Nilsson, 2012). This variation greatly affects optical parameters and visual sensation, such as the detection of different intensities, polarization and wavelengths of light to varying degrees of contrast sensitivity and acuity (Land and Nilsson, 2012). Compound eyes vary in the size and/or number of ommatidia: wider ommatidia capture more light, which can increase contrast sensitivity; however, larger interommatidial angles can lead to decreased acuity (Land, 1997; Land and Nilsson, 2012). Conversely, having many small ommatidia with narrow interommatidial angles can enhance acuity, but this may decrease contrast sensitivity (Currea et al., 2018; Palavalli-Nettimi and Theobald, 2020; Warrant, 1999, 2006). Differences in ommatidia number and size, as well as trade-offs between these structural features of compound eyes, have been described for a range of different insects (Duncan et al., 2020; Gonzalez-Bellido et al., 2011; Horridge, 1977; Posnien et al., 2012; Wakakuwa et al., 2007). Furthermore, variation in ommatidia size across the eye within species is also widely documented (Land, 1989). This size variation demonstrates areas of regional specialisation, where different visual tasks are performed by different parts of the eye. For example, killer flies, *Coenosia* sp., have evolved wider, flattened, anterior ommatidia to maximise contrast sensitivity and acuity as an adaptation to hunting (Gonzalez-Bellido et al., 2011). A number of studies have also found extensive variation in eye size within and between closely related species of *Drosophila,* caused by differences in ommatidia number and/or ommatidia area (Arif et al., 2013; Buchberger et al., 2021; Gaspar et al., 2020; Hilbrant et al., 2014; Keesey et al., 2019; Norry and Gomez, 2017; Posnien et al., 2012; Ramaekers et al., 2019; Reis et al., 2020). Despite the pervasive variation in eye morphology and detailed knowledge about eye development in *Drosophila*

(Casares and Almudi, 2016; Casares and McGregor, 2021; Kumar, 2018), little is known about the genetic and developmental bases for variation in eye size even among *Drosophila* species with a few exceptions (e.g. Ramaekers et al., 2019).

We previously showed that *D. mauritiana* has larger eyes than *D. simulans* due to larger ommatidia rather than an increase in ommatidia number (Arif et al., 2013; Posnien et al., 2012). Quantitative trait loci (QTL) mapping of this difference identified a large-effect QTL that explains 33% of the species difference. Introgression of this X-linked region from *D. mauritiana* into *D. simulans* increased the eye size and ommatidial size of the latter species (Arif et al., 2013). Here, we combine higher resolution mapping of this previously characterised X-linked QTL, with transcriptomic analysis of eye imaginal discs of *D. simulans* and *D. mauritiana,* to identify positional candidate genes that are differentially expressed in the developing ommatidia between these two species. We then carry out ATAC-seq to compare putative regulatory regions of the candidate gene *orthodenticle* (*otd*) that may contribute to differences in ommatidia diameter between *D. mauritiana* and *D. simulans.* Our results suggest that differential regulation of *otd* results in earlier expression of this homeobox gene in *D. mauritiana* compared to *D. simulans*. We hypothesise that this heterochrony in *otd* expression and consequently longer exposure to this transcription factor (TF) in maturing ommatidia in *D. mauritiana* contributes to the development of larger ommatidia in this species.

Results

Enlarged ommatidia in *D. mauritiana*

We previously found that the larger eyes of *D. mauritiana* compared to those of *D. simulans* are caused by wider diameter of central ommatidia in the former species (Arif et al., 2013; Posnien et al., 2012). To examine whether this phenotypic difference is prevalent in all ommatidia across the eye, we imaged the eyes of these two species using synchrotron radiation micro CT (SRμCT) and measured the facet diameter of ommatidia in different regions of the eye using a 3D reconstruction of each species (Fig. 1). We corroborated that while the number of ommatidia is similar between *D. mauritiana* and *D. simulans* the former has larger facets. This is consistent across anterior, central and posterior facets but is particularly pronounced in the antero-ventral region of the eye (Fig. 1 and Suppl. Table 1) (Arif et al., 2013; Posnien et al., 2012).

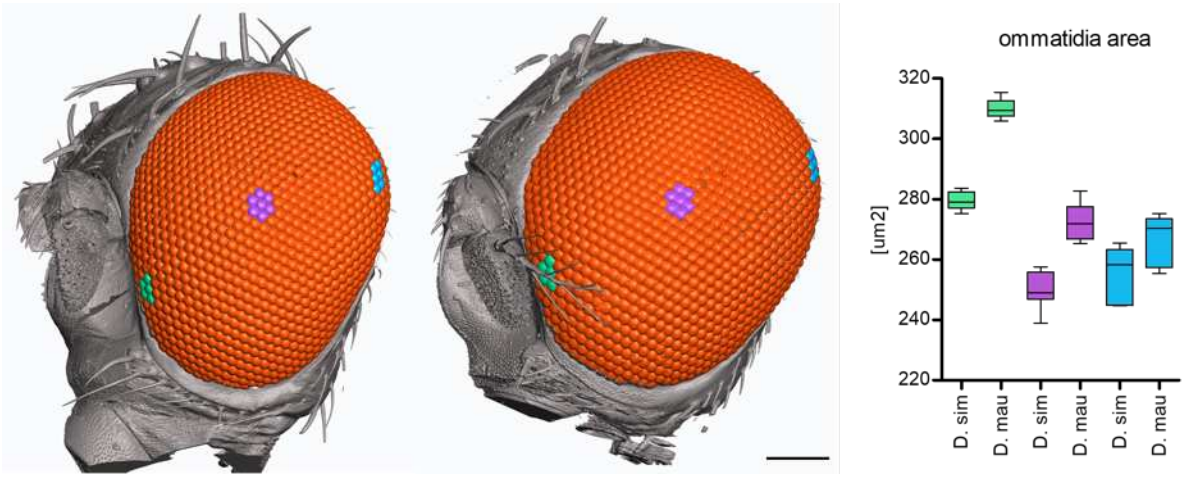

Figure 1. 3D reconstruction and ommatidia size measurements from SRμCT data of female *D. simulans* (left) and *D. mauritiana* (right). Facet areas of the ommatidia highlighted in the antero-ventral, central and dorsal-posterior region of the eye are plotted in corresponding colours (far right). Ommatidia number is 996 for the *D. simulans* and 1018 for the *D. mauritiana*. Scale bar is 100 μm.

Differentially expressed genes in a candidate region on the X chromosome

Previously we detected a QTL region located between 2.6 Mb and 8 Mb on the X chromosome, which is responsible for 33% of the difference in ommatidia size (Arif et al., 2013). Furthermore, introgression of approximately 8.3 Mb of this X-linked region (between the *yellow* (*y*) and the *vermillion* (*v*) loci) from *D. mauritiana* TAM16 into *D. simulans* YVF significantly increased the eye size of the latter, consistent with the direction of the species difference (Arif et al., 2013). Further analysis of recombinant males with breakpoints within the introgressed region revealed significant genotype-phenotype associations towards the distal end of the introgressed region near marker *v*, providing a conservative interval of about 2 Mb wherein the X QTL is likely to reside (Fig. 2a). To map the candidate region to higher resolution we generated introgression lines with breakpoints in the 2 Mb interval and compared eye area and central ommatidia diameter of y*f* male progeny (with some *D. mauritiana* DNA in the 2Mb interval) to that of their *yvf* sibling males (*i.e.*, without *D. mauritiana* DNA). We found that *yf* males had significantly larger eye size than their *yvf* siblings in introgression lines IL9.1a (one tailed t=1.80, df=11, p=.026) IL9.1b (one tailed t=1.80, df=11, p<.001) and IL9.2 (one tailed t=1.80, df=11, p=.035) but ommatidia diameter was only significantly different for IL9.1 (one tailed t=1.80, df=11, p=.014) and b (one tailed t=1.80, df=11, p=.005) (Fig. 2a). Ommatidia number and body size did not differ between y*f* males and their respective *yvf* sibling males for any of the IL lines (Suppl. Table 2). These data suggest the candidate QTL is located in a maximum region of just over 662 kb (ChrX: 7,725,195-8,387,618 in *D. simulans*).

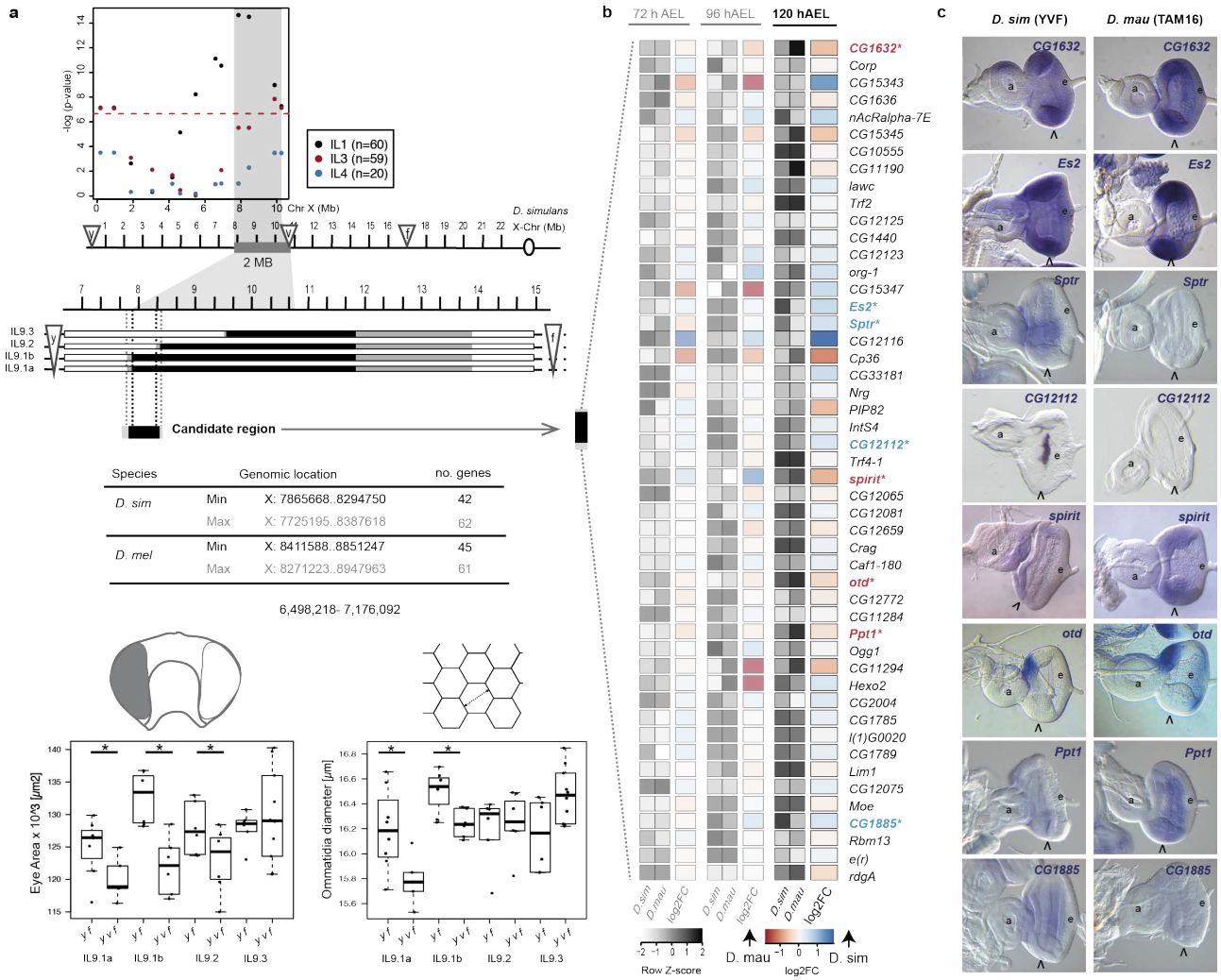

Figure 2. Differential and spatial gene expression. (a) Fine-scale mapping of X chromosome QTL. Marker-phenotype association in male recombinant progeny from three replicate introgression lines (IL1, 3, and 4, single-marker ANOVA analysis). Red dashed line indicates the Bonferroni corrected significance threshold of 0.05. Shaded grey area represents a conservative interval of ~ 2 Mb encompassing the X linked QTL. Recombination breakpoints of the new introgression lines (IL9.1-9.3) on the X chromosome (shown for *D. simulans* Flybase R2.02) define the maximum 662 kb candidate region. White, black, and grey boxes indicate DNA regions from *D. simulans* YVF, *D. mauritiana* TAM16 or not determined, respectively (the latter define the maximum candidate region). The table indicates the number of protein coding genes that are present in the candidate region in *D. simulans* and *D. melanogaster*. Distribution of eye area (left) and ommatidia diameter (right) measurements by genotype and introgression line. Asterisks indicate significance differences between genotypes where p <.05 (Suppl. Table 2). **(b)** Differential expression of 49 protein coding genes located in the introgressed region from (a) and expressed at 72 h AEL, 96 h AEL and 120 hAEL. Genes which expression is significantly higher at 120 h AEL in *D. simulans* are highlighted in blue. Genes significantly upregulated in *D. mauritiana* at 120 h AEL are shown in red. **(c)** Expression of differentially expressed genes at 120 h AEL in L3 eye-antenna imaginal discs of *D. simulans* and *D. mauritiana.* Open arrowheads indicate the MF, a: antenna, e: eye in (c).

This mapped region contains 62 protein coding positional candidate genes. To assay which positional candidates are actually expressed during the generation of

ommatidia, we performed RNA-seq experiments on the eye-antennal imaginal discs of 3rd instar larvae (L3). We extracted RNA from *D. mauritiana* and *D. simulans* eye-antennal discs at three different developmental points: at 72 hours after egg laying (AEL; late L2, at the onset of the morphogenetic furrow (MF)), when the eye primordium is proliferating and specification of the ommatidial cells has not yet started; at 96 h AEL stage (mid L3) when the MF has moved half way through the eye disc) and the most posterior ommatidia are already determined, and finally, at 120 h AEL (late L3), when the larvae are about to pupariate and most ommatidia are already determined whilst their final size, structure and shape are being arranged (Torres-Oliva et al., 2016; Torres-Oliva et al., 2018).

Comparison of the RNA-seq data among these three developmental timepoints showed that transcriptomes of 72 h AEL eye imaginal discs were the most different in comparison to transcriptomes from both 96 h AEL and 120 h AEL for both species (Suppl. Fig. 1). This reflects the distinctive processes that are occurring at these developmental stages (Torres-Oliva et al., 2018). We next focused on the expression of genes located within the mapped 0.66 Mb X-linked region and, in particular, on expression differences at 120 h AEL, when at least the most posterior ommatidia are acquiring their final size. Of the 62 genes located in this region, 49 were expressed in at least one of our RNA-seq datasets and only eight of these genes were differentially expressed between the eye discs of these two species at this timepoint (Suppl. Table 3): *spirit, otd* and *Ppt1* showed higher expression in *D. mauritiana*, whereas *CG1632, Es2, Sptr, CG12112* and *CG1885* were more highly expressed in *D. simulans* (Fig. 2b).

We next performed *in situ* hybridization experiments of these eight candidate genes to investigate if they are expressed in the eye field where the ommatidia are being assembled. These assays were carried out in both *D. mauritiana* and *D. simulans*, which allowed us to determine whether the differences in expression levels observed in the RNA-seq datasets are related to differences in spatial expression (Fig. 2c). *Sptr, CG12112* and *spirit* had no detectable expression in the relevant region posterior to the MF (Fig. 2c). *Ppt1* and *CG1885* were expressed both anterior to and immediately posterior to the MF. *CG1632* and *Es2* were ubiquitously expressed in the eye disc, with no clear regional differences. Finally, *otd* was expressed in the ocellar region of the disc and in the most posterior region of the eye field, where the ommatidia are already determined and are being assembled (Vandendries et al., 1996). *Otd* is already expressed in several rows of most posterior ommatidia of *D. mauritiana* eye discs, whereas, *otd* expression is undetectable in the most posterior regions of the eye discs of *D. simulans* (Fig. 2c). These results were consistent with our differential expression (DE) analysis, as there appeared to

be detected qualitative differences in expression levels for most of the genes investigated. Taken together, these results showed that *otd* is the only differentially expressed positional candidate gene that is expressed in maturing ommatidia (Fig. 2c).

Differences in *otd* gene expression during eye development between *D. simulans* and *D. mauritiana*

Our results suggested that *otd* transcription in the maturing ommatidia initiates earlier in *D. mauritiana* than in *D. simulans* eye discs (Fig. 2c). To investigate this further, we performed additional *in situ* hybridizations at 110 hAEL to compare the onset of *otd* expression in the developing ommatidia of these two species. At this developmental stage, we found that *otd* is already expressed in *D. mauritiana* eye discs, whereas there was no detectable expression in *D. simulans* discs (Fig. 3a-d). To confirm this heterochrony in *otd* expression we performed immunostainings against Otd protein in developing eye discs (Fig. 3e, f). We measured the number of ommatidial rows that were already specified (i.e. with positive Elav staining) as a proxy of developmental stage and then which of these ommatidial rows showed Otd expression. We observed that *D. mauritiana* discs displayed more Otd-positive ommatidia than *D. simulans* discs at the same stage (Elav positive ommatidia rows, Fig. 3e-g, Suppl. Table 4, $F_{1,47} = 30.3$, $p\text{-value}=1.48 \times 10^{-06}$). Thus, *D. mauritiana* cells in maturing ommatidia are exposed to the action of the TF Otd for longer since the expression of this protein extends into the pupal stage of both species (Suppl. Fig. 2).

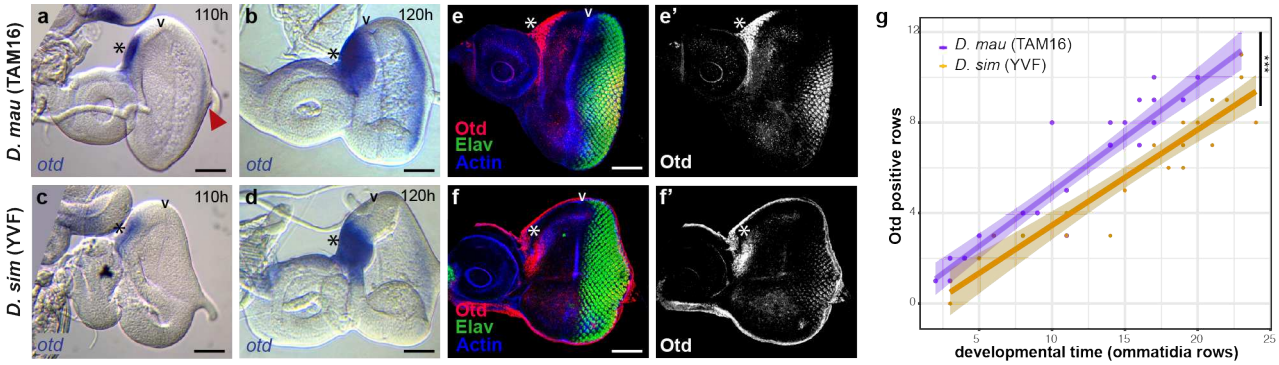

Figure 3. *otd* expression in L3 eye imaginal discs. (a-d) *otd* mRNA at 110 h AEL and 120 h AEL in *D. mauritiana* (a-b) and *D. simulans* (c-d). Arrowhead indicates the MF. Asterisks indicate expression in the ocellar region. *D. mauritiana* already exhibits *otd* mRNA at 110h (red arrowhead). **(e-f')** Immunostaining showing Otd protein (magenta, e') in mature ommatidia (marked in green by Elav) and the ocellar region (marked by an asterisk) in *D. mauritiana* (e-e') and *D. simulans* (f-f'). Staining against actin (in blue) was used to mark the MF. **(g)** Plot showing the number of Otd-positive ommatidia rows (X axis) at different developmental time points (y axis, developmental points infer by number of ommatidia rows). Asterisks represent statistical significance p< 0.001. Scale bars: 50 µm.

otd is required for the correct arrangement and size of ommatidia in _Drosophila_

It was previously shown in *D. melanogaster* that *otd* is expressed in the photoreceptor cells and is required during early pupal stages for morphogenesis of the rhabdomeres, and subsequently rhodopsin expression, as well as synaptic-column and layer targeting of these cells (Fichelson et al., 2012; Mencarelli and Pichaud, 2015; Vandendries et al., 1996). We carried out further analysis of *otd* function during eye development using RNAi knockdown and by generating mitotic clones of homozygous *otd* mutant cells. Decreasing *otd* mRNA by overexpressing *otd-miRNA* construct (Wang et al., 2010), resulted in defects in the final ommatidia organisation that were rescued by adding a copy of *UAS-otd* (Suppl. Fig. 3a-c). Loss of *otd* in clones resulted in disorganised ommatidia with perturbed shapes and sizes – often smaller than those of ommatidia of controls (Suppl. Fig. 3d). These results show that *otd* expression in the photoreceptor cells of maturing ommatidia is required for the proper regulation of ommatidial organisation and size.

Differences in chromatin accessibility in the _otd_ locus during eye development between _D. simulans_ and _D. mauritiana_

Our mapping and expression analyses indicate that the differences in *otd* expression likely contribute to differences in ommatidia size between *D. simulans* and *D. mauritiana.* Given that there is only 1 amino acid difference in the Otd sequence between our focal strains of *D. simulans* and *D. mauritiana,* our data suggest that the causative changes are located in *otd* regulatory regions. Due to the microsyntenic conservation between *D. melanogaster, D. simulans* and *D. mauritiana,* we considered the regulatory landscape of *otd* as the region between its two flanking genes, *Caf1-180* and *CG12772*, revealed by the presence of a Topological Associated Domain (TAD) in the corresponding *D. melanogaster* region (a region of 69 kb in *D. mauritiana* and 70 kb *D. simulans,* Fig. 4a, Suppl. Fig. 4; http://chorogenome.ie-freiburg.mpg.de/).

To investigate the regulation of *otd* in the developing eyes of *D. simulans* and *D. mauritiana* further, we performed ATAC-seq (Buchberger et al., 2021; Buenrostro et al., 2013; Kittelmann et al., 2018) on *D. simulans* and *D. mauritiana* eye imaginal discs at 96 and 120 h AEL. We mapped our datasets against both genomes in order to detect common, differentially accessible and species-specific regulatory regions (Fig. 4a). The ATAC-seq peak calling of the four datasets (two developmental stages and two species) revealed a total of 22 peaks in the *otd* locus, all of which were located within alignable orthologous regions in the two species (Fig. 4a).

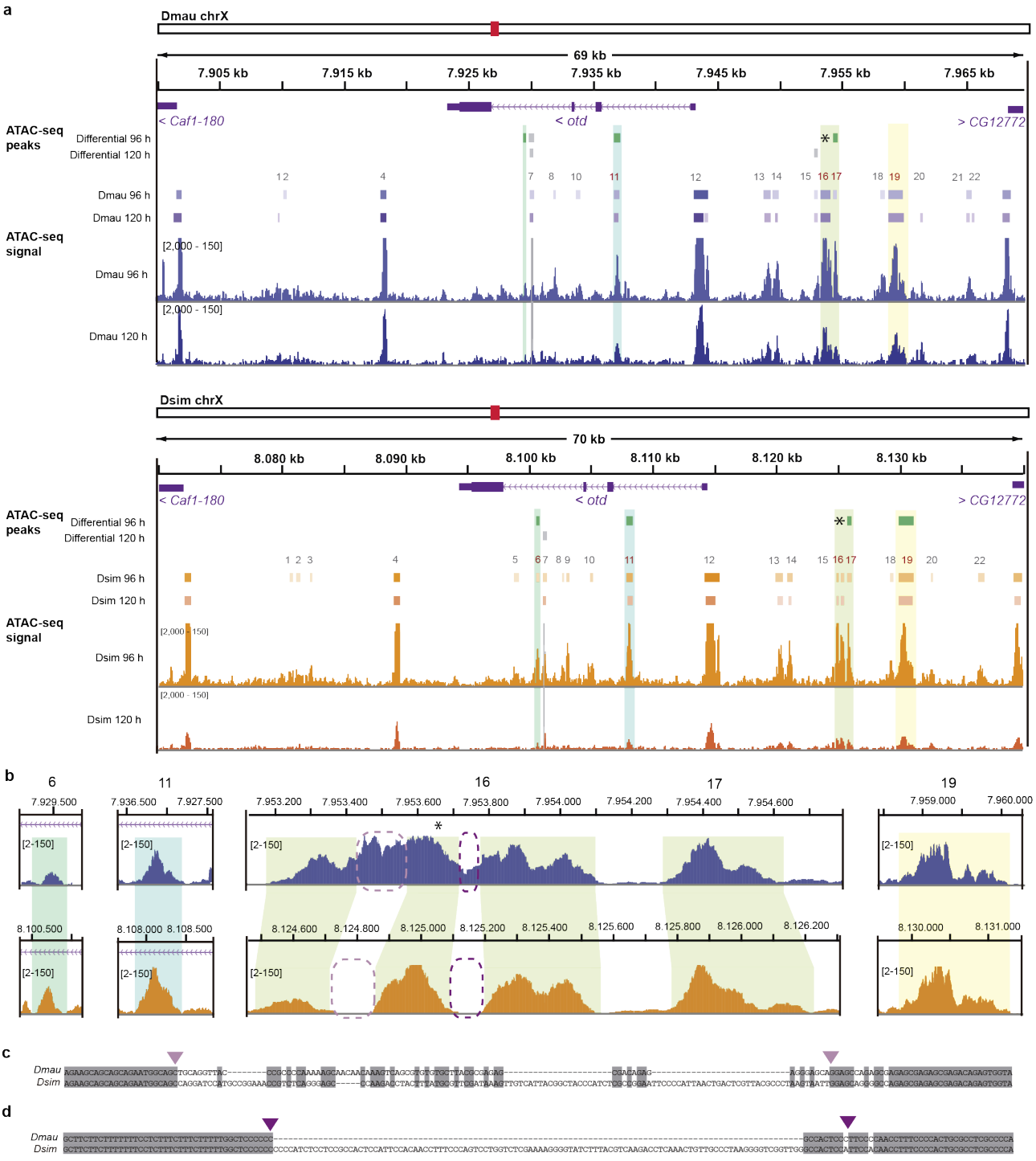

Figure 4. Chromatin accessibility at the *otd* locus. (a) Open chromatin peaks at the otd locus in 96 h AEL and 120 h AEL *D. mauritiana* and *D. simulans* eye-antenna imaginal discs. **(b)** Detail of differential peaks: 6, 11, 16, 17 and 19. **(c)** Alignment of the sequence of the first *D. mauritiana* specific region in peak 16 with *D. simulans*. **(d)** Alignment of the sequence of the second *D. mauritiana* specific region in peak 16 with *D. simulans*.

Four of these peaks showed significant differences in accessibility between *D. mauritiana* and *D. simulans*: peak 6 (*D. sim* chrX*:* 8,100,587- 8,100,808, padj = 0.00155) and peak 11 (*D. sim* chrX*:* 8,107,881-8,108,402, padj = 0.00976) in the 3rd and 1st introns of *otd,* respectively, and peaks 17 (*D. sim* chrX*:* 8,125,765 - 8,126,410, padj = 0.0418) and

19 (*D. sim* chrX*:* 8,129,876 - 8,131,170, padj = 0.0317) located upstream of *otd* (Fig. 4). We aligned the orthologous sequences of these differential peaks and found that each of them contained several sequence variants (peak 6: 8 SNPs and 2 small indels; peak 11: 8 SNPs and 5 small indels; peak 17: 4 SNPs and 1 small indel and peak 19: 29 SNPs and 4 small indels, Suppl. Fig. 5). Furthermore, we found a fifth peak (peak 16) upstream of *otd,* which did not show differential accessibility within the alignable regions, but high accessibility specifically in two *D. mauritiana* stretches that are disrupted by two insertions of 55 and 106 nucleotides respectively in *D. simulans* (Fig. 4b-d).

We next looked for transcription factor binding motifs (TFBMs) corresponding to the variant sequences within the four differential accessible peaks and in the two *D. mauritiana*-specific regions in peak 16. We predicted 164 putative TFBM in *D. simulans* and *D. mauritiana* in Peak 6 using JASPAR with a threshold of 85%. This included predicted TFBMs for Cut (Ct), Odd-paired (Opa), Optix, Sine oculis (So) and the Iroquois complex TFs (Araucan (Ara), Caupolican (Caup) and Mirror), which all have detectable expression in our RNA-seq datasets (Suppl. Table 3) and are known to be involved in eye-antennal disc development. Peak 11 encompasses 412 putative TFBMs in *D. mauritiana* and 411 putative sites in *D. simulans,* including Mad, So, Optix, Exd motifs exclusively in *D. mauritiana,* and Trl and Ttk predicted specifically in *D. simulans.* For the *D. mauritiana*-specific peak 16, 37 TFBM were predicted in the first *D. mauritiana*-specific peak (peak 16a, threshold 85%) for TFs such as Brk, Caup and Mirror, Clamp and Trl but only 8 TFBMs were predicted for the second *D. mauritiana*-specific peak (peak 16b, threshold 80%) including sites for CTCF, Mad, Brk and Trl. Peak 17 contained 269 predicted TFBMs in *D. mauritiana* and 275 predicted TFBMs in *D. simulans,* including Dichaete (D) and CTCF motifs, only present in the later species. Regarding peak 19, which covers the longest sequence, 790 and 754 TFBM were predicted for *D. mauritiana* and *D. simulans,* respectively. From those, 57 were *D. mauritiana*-specific (Eip74EF, Inv, Dll, Mirr, Al, Lim1, Vvl, Suppl. Table 5) and 60 were *D. simulans*-specific (Trl, Dll, Optix, Iroquois Complex, Dref, BEAF-32, Ems, Cut, Deaf1, E5, Ovo, Sd, Bgb::run). Overall, we identified several regions in the *otd* locus that may function as new eye enhancers for this gene in *D. mauritiana* and *D. simulans,* and that their differential activity could be responsible for the temporal differences in the onset of *otd* activation between these two species.

Differences in *otd* targets during eye development between *D. simulans* and *D. mauritiana*

Next, we investigated whether differences in the onset of expression of *otd* between *D. simulans* and *D. mauritiana* promoted further changes in its Gene Regulatory Networks (GRNs) that ultimately may be responsible for the differences in the final size of ommatidia. To this end, we called open chromatin peaks in each sample and searched for the Otd-binding motif in these accessible regions of genes expressed during eye development. Based on this analysis, we found 1,148 putative Otd target genes. We next examined which of these accessible chromatin peaks were associated with genes that were differentially expressed in our transcriptome datasets. We found that peaks associated with 161 of the 1330 genes that are upregulated in *D. mauritiana* contained Otd binding motifs, and 111 out of 1249 genes upregulated in *D. simulans* had associated peaks containing Otd binding motifs (Fig. 5a, c, Suppl. Table 6).

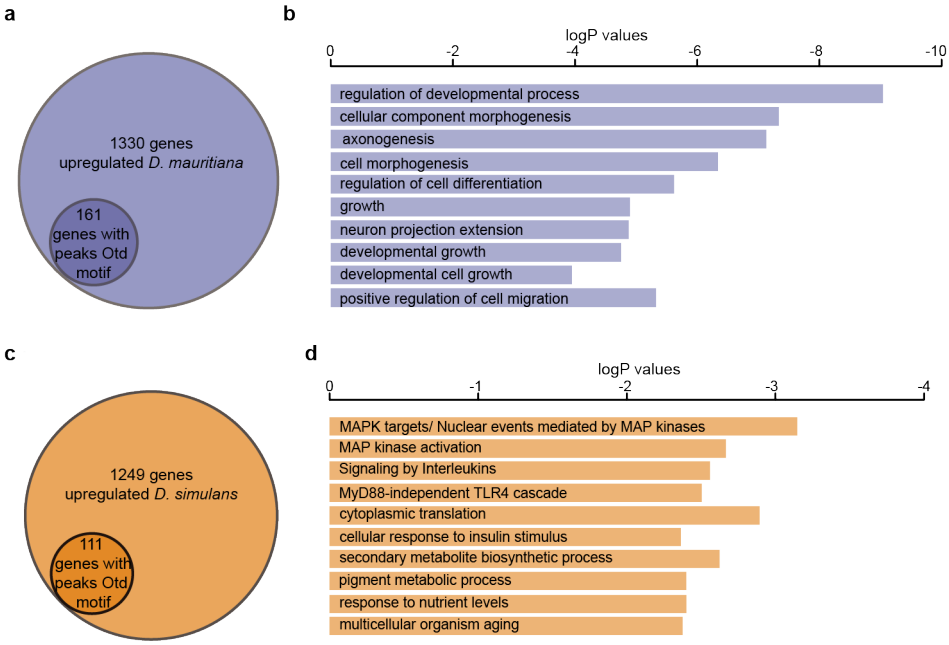

Figure 5. Otd downstream targets. (a) 161 genes upregulated in *D. mauritiana* have an associated peak that contains at least one Otd motif. **(b)** GO enrichment for those genes with Otd motifs in *D. mauritiana* **(c)** 111 genes upregulated in *D. simulans* have an associated peak that contains Otd motif. **(d)** GO enrichment for those genes with Otd motifs in *D. simulans.*

We then performed Gene Ontology (GO) term enrichment analysis for these differentially expressed genes with accessible chromatin containing Otd binding motifs. The *D. mauritiana* dataset exhibited enrichment in terms related to developmental processes, cell morphogenesis, axonogenesis, regulation of differentiation or growth, among others (Fig. 5b). By contrast, genes that were upregulated in *D. simulans* with associated Otd-peaks were enriched in terms such as the MAP kinase network, signalling by interleukins and cellular response to insulin stimulus (Fig. 5d).

Ommatidia size differences related to Rh3 expression

Given that Otd directly regulates the expression of *rh3* (Tahayato et al., 2003) and we have previously shown higher levels of *rh3* expression in adult eyes in *D. mauritiana* (Hilbrant et al., 2014; Posnien et al., 2012), we tested if the expression of Rh3 in ommatidia may have an impact on the ommatidia diameter. We used immunohistology to detect $Rh3^+$ ommatidia and applied confocal microscopy as well as 3D reconstructions to measure ommatidia in a 10x10 quadrant in the central eye region (Fig. 6a, b). This analysis showed that $Rh3^+$ ommatidia were wider in both species, while this difference was more pronounced in *D. mauritiana* (Fig. 6d). Note that we did not find differences in the ratio of $Rh3^+/Rh3^-$ ommatidia between species (Fig. 6c). This data suggested exposing maturing ommatidia longer to the action of Otd may quantitatively influence the Rh3 content, rather than the ratio of ommatidia subtypes.

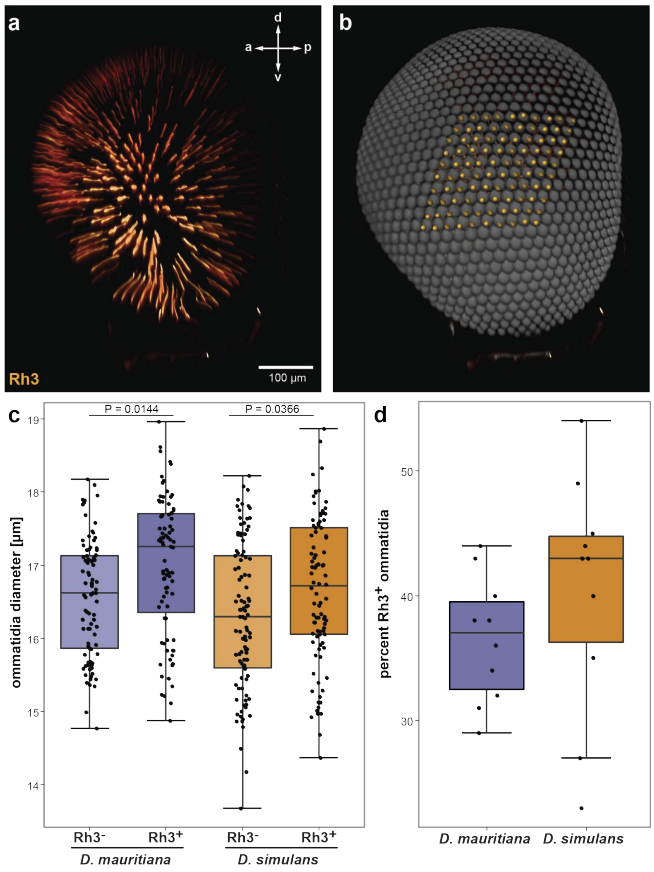

Figure 6. Differences in size of Rh3 positive ommatidia. (a) Three-dimensional reconstruction (volume rendering) of a representative *D. simulans* compound eye after clearing and cLSM imaging showing Rh3 expressing ommatidia. a – anterior, p – posterior, d – dorsal, v – ventral. **(b)** Isosurface reconstruction based on the autofluorescence (volume rendering). The 10x10 central ommatidia that were counted are labelled with yellow dots. **(c)** Boxplot showing the diameter of $Rh3^+$ and $Rh3^-$ ommatidia in both species. Differences in diameter were statistically tested applying one-way ANOVA ($F_{3,362}$ = 8.571, P = 0.0000164) followed by Tukey multiple comparisons (P-values). **(d)** Boxplot showing the percentage of $Rh3^+$ ommatidia based on the 10x10 central ommatidia counted. The differences are not significantly different (χ^2 = 3.0523, df = 1, p-value = 0.08062). The raw data for c and d are available in Suppl. Table 7**.**

Discussion

In *Drosophila*, ommatidia are produced in a posterior-to-anterior hexagonal pattern in the wake of the morphogenetic furrow (MF), which passes the presumptive retinal field during L3 to trigger photoreceptor cell specification and differentiation, and subsequently the formation of cone cells and other ommatidial cells (reviewed in (Casares and Almudi, 2016; Casares and McGregor, 2021; Gaspar et al., 2019; Kumar, 2018)). Then in pupal stages, the cone cells are placed above the photoreceptor cells and this, in combination with apoptosis and further rearrangement of pigment and other cells, produces the final number and arrangement of ommatidial cells. Final ommatidia size is specified by about 40 hours after puparium formation (hAPF), the lens is secreted from 60 hAPF, and the rhodopsins are expressed from 96 hAPF (Cagan and Ready, 1989; Earl and Britt, 2006; Kim et al., 2016).

While much is known about the specification and differentiation of ommatidia, very little is known about the regulation and evolution of their size. To investigate the genetic basis of the difference in ommatidia size between *D. mauritiana* and *D. simulans*, we carried out high-resolution introgression mapping of a previously identified X linked QTL previously mapped that explains about 33% of the difference in eye size between these two species (Arif et al., 2013). We identified eight positional candidate genes in this region that differed in expression between the developing eye-antennal discs of *D. mauritiana* and *D. simulans*. Our analysis of the spatial expression of these eight genes strongly suggests *otd* as the best candidate gene in this region for the underlying difference in ommatidia size and thus overall eye size between these species.

otd/Otx genes play several important roles during eye development in both invertebrates and vertebrates (Ragge et al., 2005; Ranade et al., 2008; Sen et al., 2013; Tahayato et al., 2003; Vandendries et al., 1996). During eye development, Otd regulates genes for cell adhesion and cytoskeletal organisation and this is essential for the correct development of the photoreceptor cells and ommatidia maturation (Fichelson et al., 2012; Ranade et al., 2008). Mutations in *otd* perturb morphogenesis of the photoreceptor cells which affects the spacing of the more apical cone cells (Fichelson et al., 2012; Vandendries et al., 1996). Intriguingly, the removal of photoreceptor cells changes ommatidia size (Miller and Cagan, 1998). We propose that although *otd* is not expressed in the lens-secreting cone cells, it indirectly affects the organisation of these cells and thus ommatidia size through regulating the maturation and organisation of the underlying photoreceptor cells. We have shown that knockdown or loss of *otd* in *D. melanogaster* perturbs ommatidia size specification, but it remains to be directly tested if variation in the

expression of this gene underlies larger and smaller ommatidia in *D. mauritiana* and *D. simulans* respectively and if *otd* contributes to the observed variation in ommatidia size in different regions of the eye.

Changes in developmental timing, or heterochrony, have played an essential role in the evolution of morphologies in multiple taxa (Alberch and Alberch, 1981; Alberch et al., 1979; Gould, 1977; McKinney, 1988). Classically, the term heterochrony has been used to refer to differences in the timing of developmental events and several examples of heterochrony have been described (Briscoe and Small, 2015; Ebisuya and Briscoe, 2018; Keyte and Smith, 2014). Most of these characterised cases showed that the mechanism responsible for the heterochrony acts downstream of its underlying genetic cause, such as changes in proliferating rates, differences in the initial size of the primordium or distinct rates of protein stability and biochemistry (Gomez et al., 2008; Kicheva et al., 2014; Matsuda et al., 2019; Rayon et al., 2020). Heterochronic shifts can also occur as direct consequence of the causative genetic change, such as those that affect regulatory regions altering the timing of gene expression (Ramaekers et al., 2019). Although differences in gene expression of single transcription factors have the potential to completely modify the subsequent GRN, the relative contribution of such direct heterochrony is in generating morphological diversity remains unknown. Our data indicate that *otd* is generally expressed more highly during ommatidial maturation in *D. mauritiana* than *D. simulans.* Further analysis shows that *otd* is actually expressed earlier during ommatidial maturation in *D. mauritiana* compared to *D. simulans.* This suggests that cis-regulatory changes in *otd* lead to ommatidial cells being exposed to Otd for longer in *D. mauritiana* resulting in larger ommatidia. Together with Ramaerkers and colleagues (Ramaekers et al., 2019), our study shows how morphological diversity in closely related species can be achieved by subtlety altering the temporal expression of a single TF. Importantly, in both cases, these transcription factors, Ey and Otd, act upstream in the GRN controlling the process, thus changes in their expression may promote major differences in downstream effectors.

Further exploration and comparison of the regulatory landscape of *otd* between *D. mauritiana* than *D. simulans* allowed us to identify several candidate cis-regulatory regions that could regulate the eye development of this gene and may contain changes that underlie the differential expression of *otd* between these two species. These regions may represent novel eye enhancers of *otd* because they do not overlap with a previously characterised eye enhancer (Hauck et al., 1999; Vandendries et al., 1996), but their activity requires further testing.

We also investigated how these changes in *otd* expression might alter target gene expression to change ommatidia size. We identified a set of genes that are differentially expressed between these two species when the ommatidia are acquiring their final size that may be acting downstream of Otd, as they have accessible chromatin regions containing putative Otd binding motifs. We compared this set of genes to known and putative targets of Otd which have been characterised later in eye development during pupal stages (Fichelson et al., 2012; Ranade et al., 2008). This comparison showed that a subset of genes for with altered expression in *otd* mutants are also differentially expressed between *D. mauritiana* and *D. simulans* in late L3. In particular, several genes involved in phototransduction (e.g. *rh3, slo, Slob, ninaG, inaD, ninaA*), genes encoding cytoskeleton and adhesion proteins (*Act88F*), and other TFs (*Dve, vnd, MED10*, etc., Suppl. Table 6). This further suggests that the network downstream of Otd varies between these two species and that ultimately, these changes in the GRN promote differences in ommatidia size between *D. mauritiana* and *D. simulans*. Intriguingly, *otd* also regulates rhodopsin expression in *D. melanogaster* (Tahayato et al., 2003), and we have shown that several rhodopsins differ in their levels and spatial expression between *D. mauritiana* and *D. simulans* (Hilbrant et al., 2014; Posnien et al., 2012). We showed that $Rh3^{+}$ ommatidia tend to be larger in diameter than $Rh3^{-}$ ommatidia. Since *rhodopsin 3* expression is higher in *D. mauritiana* (Hilbrant et al., 2014; Posnien et al., 2012) and Otd directly activates transcription of *rhodopsin 3* (Tahayato et al., 2003), a direct link between differences in *rhodopsin* expression and ommatidia diameter may exist. Therefore, it is possible that differences in *otd* expression between these two species causes differences in rhodopsin expression as well as ommatidial size, which has important implications for the vision of these flies: increased ommatidium diameter and higher rhodopsin expression could both increase photon capture, potentially resulting in greater contrast sensitivity in eyes with higher *otd* expression. Conversely, acuity is likely to be reduced due to the inherent trade-off with sensitivity. This trade-off is heavily influenced by various aspects of visual ecology, such as habitat type, circadian activity patterns, and lifestyle. Thus, substantial functional consequences with strong ecological implications could be linked to changes in the expression of a single gene such as *otd*.

Conclusions

Our data suggest that changes in the timing of *otd* expression underlie differences in ommatidia size and thus overall eye size between *D. mauritiana* and *D. simulans*. Our work provides new insights into ommatidia size regulation and the evolution of eye size.

Together with evidence from other studies showing that changes in the timing of *ey* expression contributes to differences in ommatidia number in *Drosophila* (Ramaekers et al., 2019), we now have a better understand the genetic and developmental mechanisms that underlie the large diversity in *Drosophila* eye size (Arif et al., 2013; Buchberger et al., 2021; Gaspar et al., 2020; Hilbrant et al., 2014; Keesey et al., 2019; Norry and Gomez, 2017; Posnien et al., 2012; Ramaekers et al., 2019; Reis et al., 2020). Moreover, this evidence suggests that changes in the temporal expression of upstream TFs is a widespread mechanism responsible for morphological evolution. What is also clear is the the potential this system has to build on our existing knowledge of *Drosophila* eye development (Casares and Almudi, 2016; Casares and McGregor, 2021; Domínguez and Casares, 2005; Gaspar et al., 2019; Kumar, 2018) to ultimately better understand the specification and evolution of organ size more generally.

Materials and Methods

Fly stocks and clonal analysis

D. simulans yellow (*y*), *vermillion* (*v*), *forked* (*f*) (hereafter YVF) was obtained from the *Drosophila* Species Stock Center, San Diego, California (Stock no.14021–0251.146). *D. mauritiana* TAM16 is a wild-type inbred strain. *UAS-miR-otd* and *UAS-otd* (III) were kindly provided by Henry Sun (Wang et al., 2010). *GMR-Gal4* (Hay et al., 1994) was used to drive expression of the transgenes. To generate mitotic clones of mutant *otd* in developing eyes we used the stocks *Otd[YH13], neoFRT19A/FM7c* and *RFP, neoFRT19A; ey-Flp* which were obtained from Bloomington Stock Centre (Stock nos. #8675 and #67173 respectively).

Otd mutant clones were induced in developing eyes using the Flp/FRT system. Female flies of the genotype *Otd[YH13], neoFRT19A/FM7c* were crossed with males of the genotype *RFP, neoFRT19A; ey-Flp*. Female F1 progeny were examined for the lack of the Fm7c balancer and these flies were prepared for SEM analysis (see below).

Synchrotron radiation microtomography

Fly heads were removed from the body and placed into fixative (2% PFA, 2.5% GA in 0.1 M sodium cacodylate buffer over night at 4°C. Heads were washed in water, then placed into 1% osmium tetroxide for 48 hours at 4°C, then washed and dehydrated in increasing concentrations of ethanol up to 100%. Heads were then infiltrated with increasing 812 Epon resin concentrations up to 100 % over 5 days and polymerised in embedding moulds for 24 hrs at 70°C.

Heads were scanned at the TOMCAT beamline of the Swiss Light Source (Paul Scherrer Institute, Switzerland; (Stampanoni et al., 2006). Scans were performed using a 16 keV monochromatic beam with a 20 µm LuAG:Ce scintillator. Resin blocks were trimmed and mounted using soft wax and scanned using 20x combined magnification (effective pixel size 325 nm) and a propagation distance of 25 mm. Two thousand projections were taken as the heads rotated through 180°, each with 200 ms exposure. Projections were reconstructed into 8-bit tiff stacks and Paganin filtered (delta = 1^{-8}, beta = 2^{-9}; (Paganin et al., 2002) using custom in-house software (Marone and Stampanoni, 2012). Tiff stacks were segmented in Amira (v2019.2, Thermo Fisher) for measurements of facet diameter.

SEM microscopy

Fly heads were fixed in Bouin's for 2 hours. After 2 hrs, 1/3 of total volume was replaced by 100% ethanol to fully immerse heads in Bouin's and left to fix overnight. Heads were washed and dehydrated 2x 70% EtOH overnight, 2x in 100% ethanol and finally critical point dried and mounted onto sticky carbon tabs on SEM stubs, gold coated and imaged in a Hitachi S-3400N SEM with secondary electrons at 5kV.

Markers and Introgression lines

Males were collected at backcross 7 of three replicate introgression lines (IL1, IL3 and IL4) that were recombinant within the introgressed region (males with phenotypes: *yf* or *vf*). These individuals were genotyped with eleven new additional markers (Suppl. Table 2). Significant association between each marker and eye size was tested (F-test, type III sum of squares SS) by performing a single-marker ANOVA on the residuals of eye area regressed onto T1 tibia length for each replicate (introgression line (IL 1,3 and 4; n = 20 – 60, Suppl. Table 2). Multiple testing was corrected for using Bonferroni correction. All ANOVA models were fitted in the R statistical environment (R Development Core Team 2012) using the CAR package (Fox and Weisberg, 2010).

To narrow down the 2 Mb region the X chromosome region between *y* and *v* from *D. mauritiana* TAM16 into *D. simulans* YVF was re-introgressed as in (Arif et al., 2013) *yf* females were backcrossed from multiple replicate lines to *yvf* males for a further nine generations and the end of the egg-laying cycle of that generation, we collected mothers and genotyped them for molecular markers located in the 2 Mb region (Suppl. Table 2). Four mothers with breakpoints within this region were identified. Two of them were siblings (IL9.1a and IL9.1b) and they had the same 4th great-grandmother as IL9.3 and the same

7th great-grandmother as IL9.2. Male progeny available for each of these females was collected and genotyped and phenotyped for eye area, ommatidia diameter, ommatidia number and T1 tibia length as described previously in Posnien *et al.* (Posnien et al., 2012)(Suppl. Table 2). To determine if the *D. mauritiana* DNA in the 2 Mb region resulted in larger eyes and larger ommatidia, y*f* males (with some *D. mauritiana* DNA in the 2Mb interval) were compared to that of their *yvf* sibling males (*i.e.*, without *D. mauritiana* DNA) for each introgression line using one-tailed two-sample equal-variance t-tests.

Rh3 related ommatidia measurements

Flies of both species were raised at 25°C with a 12h:12h and dark:light cycle and 40-60% humidity. Density was controlled by transferring 30-40 larvae 20-22 hours after egg laying into fresh food vials. All measurements were performed using female flies 3-5 days after eclosion.

Adult flies were decapitated and heads were cut in half. The halves were fixated in 4% paraformaldehyde (PFA) for 2-3 days. The specimens were washed three times with PBS-T (1xPBS+0.3% Triton X-100) for 10 minutes each. Afterwards they were incubated in 5% H_2O_2 for 1 day and subsequently in 10% H_2O_2 for 3-4 days until the heads were depigmented. The depigmented heads were washed three times with PBS (10X: 1.37 M NaCl, 27 mM KCl, 100mM Na_2HPO_4, 18mM KH_2PO_4) for 10 minutes each and prepared for immunostaining by incubating them in blocking solution (PBS-T+0.2% goat serum) for 4 hours. The heads were incubated for 48 hrs with the primary antibody (mouse α-Rh3; 1:10 dilution in blocking solution) and then washed five times with PBS for 1 hr each. The secondary antibodies (goat α-mouse Alexa Fluor 555; 1:1000 in blocking solution or goat α-mouse Alexa Flour 647; 1:500 in blocking solution) were applied 48 hours before the heads were washed 3 times with PBS for 10 minutes each. Subsequently, the heads were dehydrated in a graded ethanol series for 30 minutes (30%, 50%, 70%, 90%, 95% and 3 times 100% ethanol in water, respectively) and stored in 100% ethanol. For imaging heads were incubated in methyl-salicylate for 1 hour and then mounted on a cover slip with the eyes facing upwards and imaged with a cLSM (Zeiss LSM 710). The autofluorescence signal was recorded at 488 nm and the staining at 555 nm or 647 nm, respectively.

After acquisition of z-stacks using the cLSM, the data were split into the two channels, converted into tiff-files using Fiji (Image J 1.52n) and analyzed using the 3D image processing program Amira (version 5.4.1). To ensure an accurate three-dimensional representation of the data, the voxel size in the z-direction was set to 1.523 to match the refractive index of the cover slips (D 263 M borosilicate glass with refractive

index nD=1.523). Voxel sizes of x and y were entered according to the resolution of acquisition. Volume renderings of the two channels were used to visualize the data and identify ommatidia that were Rh3-positive ($Rh3^+$) and those that did not express Rh3 ($Rh3^-$) (Figure 4a). Landmarks were used to label the ommatidia and the 3D-measuring tool was used to measure the diameter of the lens of each ommatidium. For landmarks and the measuring tool to work, an isosurface of the autofluorescence channel was created to provide a reference as to where in the 3D space these were placed (Figure 4b). Using this technique, ommatidia diameters of $Rh3^+$ and $Rh3^-$ ommatidia were measured in a central region of the compound eye. Also, in a central region, a quadrant of 10x10 ommatidia was defined and the number $Rh3^+$ and $Rh3^-$ ommatidia was counted (Figure 4b). All raw diameter measurements and ommatidia counts are available in the supplementary material (Suppl. Table 7).

RNA-seq

Flies were raised at 25ºC with a 12h:12h dark:light cycle and their eggs were collected in 2 h time periods. Freshly hatched L1 larvae were transferred into fresh vials in density-controlled conditions (30 freshly hatched L1 larvae per vial). Eye-antennal imaginal discs were dissected at three different developmental time points: 72 h after egg laying (AEL), 96 h AEL and 120 h AEL and stored in RNALater (Qiagen, Venlo, Netherlands). Three biological replicates for each sample were generated. Total RNA was isolated using RNeasy Mini Kit (Qiagen). RNA quality was determined using the Agilent 2100 Bioanalyzer (Agilent Technologies, Santa Clara, CA, USA) microfluidic electrophoresis.

Library preparation for RNA-seq was performed using the TruSeq RNA Sample Preparation Kit (Illumina, catalog ID RS-122-2002) starting from 500 ng of total RNA. Accurate quantitation of cDNA libraries was performed using the QuantiFluor™dsDNA System (Promega, Madison, Wisconsin, USA). The size range of final cDNA libraries was determined by applying the DNA 1000 chip on the Bioanalyzer 2100 from Agilent (280 bp). cDNA libraries were amplified and sequenced using cBot and HiSeq 2000 (Illumina): only 120h eye-antennal imaginal disc samples were sequenced as paired-end (PE) reads (2 x 100 bp), all the rest of samples were sequenced in single-end (SE) reads (1 x 50 bp). Sequence images were transformed to bcl files using the software BaseCaller (Illumina). The bcl files were demultiplexed to fastq files with CASAVA (version 1.8.2).

Quality control analysis using FastQC software (version 0.10.1, Babraham Bioinformatics) was performed. All RNAseq reads are accessible in the Short Read Archive through umbrella BioProject PRJNA666691 (containing PRJNA374838 and

PRJNA666524). Before the mapping step, PE 100 bp reads were converted into SE 50 bp by splitting the reads in half and merging right and left reads into a single file.

The reciprocally re-annotated references described in (Torres-Oliva et al., 2016) were used to map the species-specific reads. Bowtie2 (Langmead and Salzberg, 2012) was used to map the reads to each reference (–very-sensitive-local –N 1) and the idxstats command from SAMtools v0.1.19 (Li et al., 2009) was used to summarize the number of mapped reads. HTSFilter (Rau et al., 2013) was used with default parameters to filter out genes with very low expression in all samples. For the remaining genes in each pair-wise comparison, differential expression was calculated using DESeq2 v1.2.7. with default parameters (Love et al., 2014).

ATAC-seq library preparation and sequencing

Samples were obtained following the same procedure as for the RNA-seq experiments: flies were raised at 25° C with a 12h:12h and dark:light cycle. Freshly hatched L1 larvae were transferred into vials with density-controlled conditions. Eye-antennal imaginal discs were dissected at 96 h AEL and 120 h AEL and maintained in ice cold PBS. Imaginal disc cells were lysed in 50 µl Lysis Buffer (10 mM Tris-HCl, pH = 7.5; 10 mM NaCl; 3 mM $MgCl_2$; 0.1% IGEPAL). Nuclei were collected by centrifugation at 500 g for 5 min. 75,000 nuclei were suspended in 50 µl Tagmentation Mix [25 µl Buffer (20 mM Tris- CH_3COO^-, pH = 7.6; 10 mM $MgCl_2$; 20% Dimethylformamide); 2.5 µl Tn5 Transposase; 22.5 µl H_2O] and incubated at 37℃ for 30 min. After addition of 3 µl 2 M NaAC, pH = 5.2 DNA was purified using a QIAGEN MinElute Kit. PCR amplification for library preparation was done for 14 cycles with NEBNext High Fidelity Kit; primers were used according to (Buenrostro et al., 2013). Paired end 50 bp sequencing was carried out by the Transcriptome and Genome Analysis Laboratory Goettingen, Germany.

ATACseq peak calling and differential binding site analysis

ATAC-seq raw reads were generated from the following samples (2 replicates each): *D. simulans* larvae at 96h AEL and 120h AEL and *D. mauritiana* larvae at 96h AEL and 120h AEL. These reads were mapped to strain-specific genomes of *D. mauritiana* and *D. simulans* (Torres-Oliva et al., 2016) using Bowtie2 (version 2.3.4.1) (Langmead and Salzberg, 2012) with the parameter –X2000. The Samtools suite v0.1.19 (Li et al., 2009) was used to convert *.sam to *.bam files and to further process the mapped reads. Duplicates were removed using Picard (version 2.20.2) with the parameter

REMOVE_DUPLICATE=TRUE. Bam files were then converted to bed files using the Bedtools (version 2.24) bamtobed command. Reads were centred according to (Buenrostro et al., 2013). These reads were then converted to the *D. melanogaster* coordinate system using liftOver (1.14.0) with custom prepared chain files, one for the conversion of *D. mauritiana* coordinates to *D. melanogaster* coordinates and one for the conversion of *D. simulans* coordinates to *D. melanogaster* coordinates. Peaks were then called using MACS2 (version 2.1.2, (Zhang et al., 2008)) with the following parameters: --shift – 100, extsize 200, -q 0.01.

We used the Diffbind package (version 2.12.0, (Ross-Innes et al., 2012)) in R (version 3.6.1.) to search for differentially accessible ATAC-seq regions. A consensus peak set of 19,872 peaks (96h AEL) and 15,868 peaks (120h AEL) was used for all samples and the reads were counted for each identified peak with the dba.count command. For each time point separately we used the dba.analyze command with default parameters to get differentially accessible peaks between the two species. This command uses by default the DESeq2 analysis. All plots were as well generated with the DiffBind package.

To search for TFBM of potential *otd* regulators, we used the JASPAR core database and its online tool for screening DNA sequences of ATAC-seq peaks with all possible TFB motifs from insects (153 profiles) with a relative profile score threshold of 85%.

Gene regulatory network reconstruction

To search for TFBM of potential *otd* regulators, we used the JASPAR core database and its online tool for screening DNA sequences of ATAC-seq peaks in the *otd* locus (between the two flanking genes) with all possible TFB motifs from insects (153 profiles) with a relative profile score threshold of 90%.

To define a list of potential Otd target genes, we used an Otd-motif (Dmelanogaster-FlyFactorSurvey-Oc_Cell_FBgn0004102) from the MotifDB package (version 1.16.1), which provides a collection of available transcription factors in R (version 3.3.3). We searched for Otd binding sites in accesible chromatin regions with the findMotifsGenome.pl command implemented in the HOMER (version V4.10.4, (Heinz et al., 2010)) in all samples. All peaks with a predicted Otd motif were annotated to an associated gene using the annotatePeaks.pl command by HOMER and combined all time points and both species into one file. We then looked for the number of genes with an annotated Otd motif and found 1,148 unique genes, which we overlapped with our RNA-

seq dataset to find out which of these target genes were differentially expressed between the two species. GO term enrichment analysis of putative Otd target genes was performed using the online tool Metascape (Zhou et al., 2019).

We used the online STRING database that integrates all known and predicted associations between proteins based on evidence from a variety of sources (Szklarczyk et al., 2020), to construct networks of DEG encoded proteins. To visualize the network and map genes/prot with Otd motifs we applied the Cytoscape software (Shannon et al., 2003).

In situ hybridisation and immunohistochemistry

In situ hybridizations were carried out using a standard protocol with DIG-labeled antisense RNA probes. Eye-antenna imaginal discs were dissected and fixed at 120 h AEL for 40 min in 4% formaldehyde. To be able to compare the expression patterns avoiding technical differences (i.e. probe affinity and probe concentration), we first aligned the sequences from *D. mauritiana* and *D. simulans* and designed RNA probes within fragments with at least 95% of similarity between them (Suppl. Table 8). This design allowed us to perform the *in situ* hybridization experiments using the same specific probes for each of the candidate genes at the same concentration for both species. The nitro blue tetrazolium/5-bromo-4-chloro-3′-indolyphosphate (NBT-BCIP) reaction was stopped at the same time. Candidate gene sequences were cloned into a TOPO PCR4 (*spirit, otd*, *Ppt1, CG1632, Es2* and *CG12112*) or pCRII (*CG1885, Sptr*) vectors (Invitrogen) using specific primer pairs (Suppl. Table 8), respectively, following the manufacturer's protocol. M13 forward and reverse primers were used to linearize the DNA. According to the vector and orientation of the fragments T3, T7 or SP6 RNA polymerase were used to generate the DIG-labeled riboprobes.

Immunostainings with Rabbit anti-Otd (Wang et al., 2010) and rat anti-Elav (7E8A10, Hybridoma bank) were performed at 1:1500 and 1:100 dilutions respectively using standard protocols, followed by anti-rat-Cy3 (Jackson Immuno Research) and anti-rabbit-Alexafluor 647 (Molecular probes) secondary AB staining, at 1:200. The actin cytoskeleton was stained with Alexafluor 488-Phalloidin (Molecular Probes) at 1:40 dilution for 30 min after discs fixation. Discs were mounted in Prolong Gold antifade reagent, supplemented with DAPI (Molecular Probes), and captured with a Zeiss LSM 510 confocal microscope. Images were processed using NIH ImageJ software.

706 **Otd positive cells measurements**

707 We used an Analysis of Covariance (ANCOVA) to test for differences between strains for
708 Otd-positive ommatidia while adjusting for differences in development stage by using the
709 number of ommatidial rows as a proxy for the latter. The ANCOVA was performed using
710 base R v4.0.2 (R Core Team, 2020).

711

712 **Data Availability**

713 All RNAseq and ATACseq reads are accessible in the Short Read Archive through
714 umbrella BioProject PRJNA666691 (containing PRJNA374838 and PRJNA666524).

715

716 **Acknowledgements**

717 This work was funded by grants from the ERC (242553) to A.P.M. and BBSRC
718 (BB/M020967/1, BB/T000317/1) to A.P.M. and I.A. and A.P.M. and M.K respectively. M.T.-
719 O. was supported by a “la Caixa-DAAD” fellowship. N.P. and E.B. were funded by the
720 Deutsche Forschungsgesellschaft (DFG, Grant No. PO 1648/3-1 to N.P.). We
721 acknowledge the Paul Scherrer Institut, Villigen, Switzerland for provision of synchrotron
722 radiation beamtime at the TOMCAT beamline X02DA of the SLS, and the invaluable
723 assistance of Dr Christian Schlepütz. We want to thank the Transcriptome and Genome
724 Core Unit, University Medical Center Göttingen (UMG) for support with next generation
725 sequencing and Franck Pichaud for giving us access to *otd* microarray data.

Supplementary Files

Supplementary Figure 1. RNA-seq datasets.

Supplementary Figure 2. *otd* expression in pupal eyes.

Supplementary Figure 3. Loss of *otd* causes defects in ommatidia structure.

Supplementary Figure 4. Topological Domain Associated with *otd* locus in *D. melanogaster*

Supplementary Figure 5. Alignment of differential open chromatin regions in the *otd* locus of *D. simulans* and *D. mauritiana*

Supplementary Table 1. Measurements of ommatidia size of *D. mauritiana* and *D. simulans* eyes

Supplementary Table 2. Mapping and introgression data

Supplementary Table 3 Pair-wise differential expression analysis (D.sim vs. D.mau) results for each time point (72h, 96h and 120h).

Supplementary Table 4. Measurements of Otd-positive ommatidia in *D. mauritiana* and *D. simulans* eye discs

Supplementary Table 5. TFBM in differential open chromatin regions in *otd* locus of *D. simulans* and *D. mauritiana*

Supplementary Table 6. Differentially expressed genes with predicted Otd TFBMs in their associated open chromatin regions.

Supplementary Table 7. Raw data of diameter measurements of $Rh3^{+}$ and $Rh3^{-}$ ommatidia and the ratio of $Rh3^{+}/Rh3^{-}$ ommatidia.

Supplementary Table 8. Primers used to generate probes for in situ hybridization

761 **References**

762

763 Alberch, P., Alberch, J., 1981. Heterochronic mechanisms of morphological diversification and
764 evolutionary change in the neotropical salamander, Bolitoglossa occidentalis (Amphibia:
765 Plethodontidae). Journal of Morphology 167, 249-264.

766 Alberch, P., Gould, S.J., Oster, G.F., Wake, D.B., 1979. Size and Shape in Ontogeny and
767 Phylogeny. Paleobiology 5, 296-317.

768 Arif, S., Hilbrant, M., Hopfen, C., Almudi, I., Nunes, M.D., Posnien, N., Kuncheria, L., Tanaka, K.,
769 Mitteroecker, P., Schlotterer, C., McGregor, A.P., 2013. Genetic and developmental analysis of
770 differences in eye and face morphology between Drosophila simulans and Drosophila mauritiana.
771 Evol Dev 15, 257-267.

772 Arnoult, L., Su, K.F.Y., Manoel, D., Minervino, C., Magriña, J., Gompel, N., Prud'homme, B., 2013.
773 Emergence and Diversification of Fly Pigmentation Through Evolution of a Gene Regulatory
774 Module. Science 339, 1423-1426.

775 Briscoe, J., Small, S., 2015. Morphogen rules: design principles of gradient-mediated embryo
776 patterning. Development 142, 3996-4009.

777 Buchberger, E., Bilen, A., Ayaz, S., Salamanca, D., Matas de las Heras, C., Niksic, A., Almudi, I.,
778 Torres-Oliva, M., Casares, F., Posnien, N., 2021. Variation in pleiotropic hub gene expression is
779 associated with interspecific differences in head shape and eye size in Drosophila. Molecular
780 Biology and Evolution.

781 Buenrostro, J.D., Giresi, P.G., Zaba, L.C., Chang, H.Y., Greenleaf, W.J., 2013. Transposition of
782 native chromatin for fast and sensitive epigenomic profiling of open chromatin, DNA-binding
783 proteins and nucleosome position. Nat Methods 10, 1213-1218.

784 Cagan, R.L., Ready, D.F., 1989. The emergence of order in the Drosophila pupal retina. Dev Biol
785 136, 346-362.

786 Casares, F., Almudi, I., 2016. Fast and Furious 800. The Retinal Determination Gene Network in
787 Drosophila, in: Castelli-Gair Hombría, J., Bovolenta, P. (Eds.), Organogenetic Gene Networks:
788 Genetic Control of Organ Formation. Springer International Publishing, Cham, pp. 95-124.

789 Casares, F., McGregor, A.P., 2021. The evolution and development of eye size in flies. WIREs
790 Developmental Biology n/a, e380.

791 Courtier-Orgogozo, V., Arnoult, L., Prigent, S.R., Wiltgen, S., Martin, A., 2019. Gephebase, a
792 database of genotype–phenotype relationships for natural and domesticated variation in
793 Eukaryotes. Nucleic Acids Research 48, D696-D703.

794 Currea, J.P., Smith, J.L., Theobald, J.C., 2018. Small fruit flies sacrifice temporal acuity to maintain
795 contrast sensitivity. Vision Res 149, 1-8.

796 Domínguez, M., Casares, F., 2005. Organ specification-growth control connection: new in-sights
797 from the Drosophila eye-antennal disc. Dev Dyn 232, 673-684.

798 Duncan, A.B., Salazar, B.A., Garcia, S.R., Brandley, N.C., 2020. A sexual dimorphism in the
799 spatial vision of band-winged grasshoppers. bioRxiv, 2020.2009.2018.303784.

800 Earl, J.B., Britt, S.G., 2006. Expression of Drosophila rhodopsins during photoreceptor cell
801 differentiation: insights into R7 and R8 cell subtype commitment. Gene Expr Patterns 6, 687-694.

802 Ebisuya, M., Briscoe, J., 2018. What does time mean in development? Development 145.

803 Fichelson, P., Brigui, A., Pichaud, F., 2012. Orthodenticle and Kruppel homolog 1 regulate
804 Drosophila photoreceptor maturation. Proc Natl Acad Sci U S A 109, 7893-7898.

805 Fox, J., Weisberg, S., 2010. An R Companion to Applied Regression. SAGE Publications, Inc.

806 Gaspar, P., Almudi, I., Nunes, M.D.S., McGregor, A.P., 2019. Human eye conditions: insights from
807 the fly eye. Hum Genet 138, 973-991.

808 Gaspar, P., Arif, S., Sumner-Rooney, L., Kittelmann, M., Bodey, A.J., Stern, D.L., Nunes, M.D.S.,
809 McGregor, A.P., 2020. Characterization of the Genetic Architecture Underlying Eye Size Variation
810 Within Drosophila melanogaster and Drosophila simulans. G3 (Bethesda) 10, 1005-1018.

811 Gomez, C., Özbudak, E.M., Wunderlich, J., Baumann, D., Lewis, J., Pourquié, O., 2008. Control of
812 segment number in vertebrate embryos. Nature 454, 335-339.

813 Gonzalez-Bellido, P.T., Wardill, T.J., Juusola, M., 2011. Compound eyes and retinal information
814 processing in miniature dipteran species match their specific ecological demands. Proc Natl Acad
815 Sci U S A 108, 4224-4229.

816 Gould, S.J., 1977. Ontogeny and Phylogeny. Cambridge, Mass. ;. Belknap Press of Harvard
817 University Press,.

818 Hagen, J.F.D., Mendes, C.C., Blogg, A., Payne, A., Tanaka, K.M., Gaspar, P., Figueras Jimenez,
819 J., Kittelmann, M., McGregor, A.P., Nunes, M.D.S., 2019. tartan underlies the

evolution of Drosophila male genital morphology. Proceedings of the National Academy of Sciences 116, 19025-19030.

Hauck, B., Gehring, W.J., Walldorf, U., 1999. Functional analysis of an eye specific enhancer of the eyeless gene in Drosophila. Proceedings of the National Academy of Sciences of the United States of America 96, 564-569.

Hay, B.A., Wolff, T., Rubin, G.M., 1994. Expression of baculovirus P35 prevents cell death in Drosophila. Development 120, 2121-2129.

Heinz, S., Benner, C., Spann, N., Bertolino, E., Lin, Y.C., Laslo, P., Cheng, J.X., Murre, C., Singh, H., Glass, C.K., 2010. Simple Combinations of Lineage-Determining Transcription Factors Prime cis-Regulatory Elements Required for Macrophage and B Cell Identities. Molecular Cell 38, 576-589.

Hilbrant, M., Almudi, I., Leite, D.J., Kuncheria, L., Posnien, N., Nunes, M.D., McGregor, A.P., 2014. Sexual dimorphism and natural variation within and among species in the Drosophila retinal mosaic. BMC Evol Biol 14, 240.

Horridge, G.A., 1977. The Compound Eye of Insects. Scientific American 237, 108-121.

Keesey, I.W., Grabe, V., Gruber, L., Koerte, S., Obiero, G.F., Bolton, G., Khallaf, M.A., Kunert, G., Lavista-Llanos, S., Valenzano, D.R., Rybak, J., Barrett, B.A., Knaden, M., Hansson, B.S., 2019. Inverse resource allocation between vision and olfaction across the genus Drosophila. Nat Commun 10, 1162.

Keyte, A.L., Smith, K.K., 2014. Heterochrony and developmental timing mechanisms: changing ontogenies in evolution. Semin Cell Dev Biol 34, 99-107.

Kicheva, A., Bollenbach, T., Ribeiro, A., Valle, H.P., Lovell-Badge, R., Episkopou, V., Briscoe, J., 2014. Coordination of progenitor specification and growth in mouse and chick spinal cord. Science 345, 1254927.

Kim, S., Cassidy, J.J., Yang, B., Carthew, R.W., Hilgenfeldt, S., 2016. Hexagonal Patterning of the Insect Compound Eye: Facet Area Variation, Defects, and Disorder. Biophys J 111, 2735-2746.

Kittelmann, S., Buffry, A.D., Franke, F.A., Almudi, I., Yoth, M., Sabaris, G., Couso, J.P., Nunes, M.D.S., Frankel, N., Gomez-Skarmeta, J.L., Pueyo-Marques, J., Arif, S., McGregor, A.P., 2018. Gene regulatory network architecture in different developmental contexts influences the genetic basis of morphological evolution. PLoS Genet 14, e1007375.

850 Klaassen, H., Wang, Y., Adamski, K., Rohner, N., Kowalko, J.E., 2018. CRISPR mutagenesis
851 confirms the role of oca2 in melanin pigmentation in Astyanax mexicanus. Dev Biol 441, 313-318.

852 Kumar, J.P., 2018. The fly eye: Through the looking glass. Developmental Dynamics 247, 111-
853 123.

854 Land, M.F., 1989. Variations in the Structure and Design of Compound Eyes. Springer Berlin
855 Heidelberg, Berlin, Heidelberg, pp. 90-111.

856 Land, M.F., 1997. Visual acuity in insects. Annu Rev Entomol 42, 147-177.

857 Land, M.F., Nilsson, D., 2012. Animal eyes. Oxford University Press, Oxford.

858 Langmead, B., Salzberg, S.L., 2012. Fast gapped-read alignment with Bowtie 2. Nat Methods 9,
859 357-359.

860 Li, H., Handsaker, B., Wysoker, A., Fennell, T., Ruan, J., Homer, N., Marth, G., Abecasis, G.,
861 Durbin, R., Subgroup, G.P.D.P., 2009. The Sequence Alignment/Map format and SAMtools.
862 Bioinformatics 25, 2078-2079.

863 Love, M.I., Huber, W., Anders, S., 2014. Moderated estimation of fold change and dispersion for
864 RNA-seq data with DESeq2. Genome Biology 15, 550.

865 Marone, F., Stampanoni, M., 2012. Regridding reconstruction algorithm for real-time tomographic
866 imaging. J Synchrotron Radiat 19, 1029-1037.

867 Matsuda, M., Hayashi, H., Garcia-Ojalvo, J., Yoshioka-Kobayashi, K., Kageyama, R., Yamanaka,
868 Y., Ikeya, M., Toguchida, J., Alev, C., Ebisuya, M., 2019. Species-specific oscillation periods of
869 human and mouse segmentation clocks are due to cell autonomous differences in biochemical
870 reaction parameters. bioRxiv, 650648.

871 McKinney, M.L., 1988. Heterochrony in Evolution, in: McKinney, M.L. (Ed.), Heterochrony in
872 Evolution: A Multidisciplinary Approach. Springer US, Boston, MA, pp. 327-340.

873 Mencarelli, C., Pichaud, F., 2015. Orthodenticle Is Required for the Expression of Principal
874 Recognition Molecules That Control Axon Targeting in the Drosophila Retina. PLoS Genet 11,
875 e1005303.

876 Miller, D.T., Cagan, R.L., 1998. Local induction of patterning and programmed cell death in the
877 developing Drosophila retina. Development 125, 2327-2335.

878 Norry, F.M., Gomez, F.H., 2017. Quantitative Trait Loci and Antagonistic Associations for Two
879 Developmentally Related Traits in the Drosophila Head. J Insect Sci 17.

880 Paganin, D., Mayo, S.C., Gureyev, T.E., Miller, P.R., Wilkins, S.W., 2002. Simultaneous phase and
881 amplitude extraction from a single defocused image of a homogeneous object. J Microsc 206, 33-
882 40.

883 Palavalli-Nettimi, R., Theobald, J.C., 2020. Small eyes in dim light: Implications to spatio-temporal
884 visual abilities in Drosophila melanogaster. Vision Res 169, 33-40.

885 Posnien, N., Hopfen, C., Hilbrant, M., Ramos-Womack, M., Murat, S., Schonauer, A., Herbert,
886 S.L., Nunes, M.D., Arif, S., Breuker, C.J., Schlotterer, C., Mitteroecker, P., McGregor, A.P., 2012.
887 Evolution of eye morphology and rhodopsin expression in the Drosophila melanogaster species
888 subgroup. PLoS One 7, e37346.

889 Ragge, N.K., Brown, A.G., Poloschek, C.M., Lorenz, B., Henderson, R.A., Clarke, M.P., Russell-
890 Eggitt, I., Fielder, A., Gerrelli, D., Martinez-Barbera, J.P., Ruddle, P., Hurst, J., Collin, J.R., Salt, A.,
891 Cooper, S.T., Thompson, P.J., Sisodiya, S.M., Williamson, K.A., Fitzpatrick, D.R., van Heyningen,
892 V., Hanson, I.M., 2005. Heterozygous mutations of OTX2 cause severe ocular malformations. Am
893 J Hum Genet 76, 1008-1022.

894 Ramaekers, A., Claeys, A., Kapun, M., Mouchel-Vielh, E., Potier, D., Weinberger, S., Grillenzoni,
895 N., Dardalhon-Cumenal, D., Yan, J., Wolf, R., Flatt, T., Buchner, E., Hassan, B.A., 2019. Altering
896 the Temporal Regulation of One Transcription Factor Drives Evolutionary Trade-Offs between
897 Head Sensory Organs. Dev Cell 50, 780-792 e787.

898 Ranade, S.S., Yang-Zhou, D., Kong, S.W., McDonald, E.C., Cook, T.A., Pignoni, F., 2008.
899 Analysis of the Otd-dependent transcriptome supports the evolutionary conservation of
900 CRX/OTX/OTD functions in flies and vertebrates. Dev Biol 315, 521-534.

901 Rau, A., Gallopin, M., Celeux, G., Jaffrezic, F., 2013. Data-based filtering for replicated high-
902 throughput transcriptome sequencing experiments. Bioinformatics 29, 2146-2152.

903 Rayon, T., Stamataki, D., Perez-Carrasco, R., Garcia-Perez, L., Barrington, C., Melchionda, M.,
904 Exelby, K., Lazaro, J., Tybulewicz, V.L.J., Fisher, E.M.C., Briscoe, J., 2020. Species-specific pace
905 of development is associated with differences in protein stability. Science 369, eaba7667.

906 Reis, M., Wiegleb, G., Claude, J., Lata, R., Horchler, B., Ha, N.-T., Reimer, C., Vieira, C.P., Vieira,
907 J., Posnien, N., 2020. Multiple loci linked to inversions are associated with eye size variation in
908 species of the Drosophila virilis phylad. Scientific Reports 10, 12832.

909 Ross-Innes, C.S., Stark, R., Teschendorff, A.E., Holmes, K.A., Ali, H.R., Dunning, M.J., Brown,
910 G.D., Gojis, O., Ellis, I.O., Green, A.R., Ali, S., Chin, S.-F., Palmieri, C., Caldas, C., Carroll, J.S.,
911 2012. Differential oestrogen receptor binding is associated with clinical outcome in breast cancer.
912 Nature 481, 389-393.

913 Santos, M.E., Le Bouquin, A., Crumière, A.J.J., Khila, A., 2017. Taxon-restricted genes at the
914 origin of a novel trait allowing access to a new environment. Science 358, 386-390.

915 Sen, S., Reichert, H., VijayRaghavan, K., 2013. Conserved roles of ems/Emx and otd/Otx genes in
916 olfactory and visual system development in Drosophila and mouse. Open Biol 3, 120177.

917 Shannon, P., Markiel, A., Ozier, O., Baliga, N.S., Wang, J.T., Ramage, D., Amin, N., Schwikowski,
918 B., Ideker, T., 2003. Cytoscape: a software environment for integrated models of biomolecular
919 interaction networks. Genome Res 13, 2498-2504.

920 Stampanoni, M., Groso, A., Isenegger, A., Mikuljan, G., Chen, Q., Bertrand, A., Henein, S.,
921 Betemps, R., Frommherz, U., Böhler, P., Meister, D., Lange, M., Abela, R., 2006. Trends in
922 synchrotron-based tomographic imaging: the SLS experience. SPIE.

923 Szklarczyk, D., Gable, A.L., Nastou, K.C., Lyon, D., Kirsch, R., Pyysalo, S., Doncheva, N.T.,
924 Legeay, M., Fang, T., Bork, P., Jensen, L.J., von Mering, C., 2020. The STRING database in 2021:
925 customizable protein–protein networks, and functional characterization of user-uploaded
926 gene/measurement sets. Nucleic Acids Research 49, D605-D612.

927 Tahayato, A., Sonneville, R., Pichaud, F., Wernet, M.F., Papatsenko, D., Beaufils, P., Cook, T.,
928 Desplan, C., 2003. Otd/Crx, a Dual Regulator for the Specification of Ommatidia Subtypes in the
929 Drosophila Retina. Developmental Cell 5, 391-402.

930 Torres-Oliva, M., Almudi, I., McGregor, A.P., Posnien, N., 2016. A robust (re-)annotation approach
931 to generate unbiased mapping references for RNA-seq-based analyses of differential expression
932 across closely related species. BMC Genomics 17, 392.

933 Torres-Oliva, M., Schneider, J., Wiegleb, G., Kaufholz, F., Posnien, N., 2018. Dynamic genome
934 wide expression profiling of Drosophila head development reveals a novel role of Hunchback in
935 retinal glia cell development and blood-brain barrier integrity. PLOS Genetics 14, e1007180.

936 Vandendries, E.R., Johnson, D., Reinke, R., 1996. orthodenticle is required for photoreceptor cell
937 development in the Drosophila eye. Dev Biol 173, 243-255.

938 Wakakuwa, M., Stavenga, D.G., Arikawa, K., 2007. Spectral Organization of Ommatidia in Flower-
939 visiting Insects†. Photochemistry and Photobiology 83, 27-34.

940 Wang, L.H., Huang, Y.T., Tsai, Y.C., Sun, Y.H., 2010. The role of eyg Pax gene in the
941 development of the head vertex in Drosophila. Dev Biol 337, 246-258.

942 Warrant, E.J., 1999. Seeing better at night: life style, eye design and the optimum strategy of
943 spatial and temporal summation. Vision Res 39, 1611-1630.

944 Warrant, E.J., 2006. Invertebrate vision in dim light,. Warrant, E.J., Nilsson, D.-E. (Eds.),
945 Invertebrate vision. Cambridge University Press, Cambridge, 83-126.

946 Zhang, Y., Liu, T., Meyer, C.A., Eeckhoute, J., Johnson, D.S., Bernstein, B.E., Nusbaum, C.,
947 Myers, R.M., Brown, M., Li, W., Liu, X.S., 2008. Model-based Analysis of ChIP-Seq (MACS).
948 Genome Biology 9, R137.

949 Zhou, Y., Zhou, B., Pache, L., Chang, M., Khodabakhshi, A.H., Tanaseichuk, O., Benner, C.,
950 Chanda, S.K., 2019. Metascape provides a biologist-oriented resource for the analysis of systems-
951 level datasets. Nature Communications 10, 1523.
952